

Fluid mode spectroscopy for measuring kinematic viscosity of fluids in open cylindrical containers

Hideshi Ishida,^{a)} Masaaki Horie, Takahiro Harada, Shingo Mizuno, Seita Hamada, Haruki Imura, Shoma Ashiwake, Naoya Isayama, Ryomei Saeki, Ryotaro Kozono, Daichi Taki, and Asuka Kurose

Department of Mechanical Engineering, Faculty of Science and Engineering, Setsunan University, 17-8 Ikeda-Nakamachi, Neyagawa, Osaka 572-8508, Japan

On a daily basis we stir tea or coffee with a spoon and leave it to rest. We know empirically the larger the stickiness, viscosity, of the fluid, more rapidly its velocity slows down. It is surprising, therefore, that the variation, the decay rate of the velocity, has not been utilized for measuring (kinematic) viscosity of fluids. This study shows that a spectroscopy decomposing a velocity field into fluid modes (Stokes eigenmodes) allows us to measure accurately the kinematic viscosity. The method, Fluid Mode Spectroscopy (FMS), is based on the fact that each Stokes eigenmode has its inherent decay rate of eigenvalue and that the dimensionless rate of the slowest decaying mode (SDM) is constant, dependent only on the normalized shape of a fluid container, obtained analytically for some shapes including cylindrical containers. The FMS supplements major conventional measuring methods with each other, particularly useful for measuring relatively low kinematic viscosity and for a direct measurement of viscosity at zero shear rate without extrapolation. The method is validated by the experiments of water poured into an open cylindrical container, as well as by the corresponding numerical simulations.

Keywords: kinematic viscosity; Stokes eigenmodes; (dimensionless) decay rate; cylindrical container

^{a)}Electronic mail: hideshi.ishida@mec.setsunan.ac.jp

I. INTRODUCTION

Since Isaac Newton stated in 1687 that the resistance in the parts of a fluid is proportional to the velocity with which the parts of the fluid are separated from one another¹, viscosity has been an important physical quantity in fluid mechanics and engineering. However, it took nearly 200 years for viscosity to be measured until the dynamical equation of fluid was established^{2,3}.

To our best knowledge, Hagenbach was the first in the world to measure viscosity and report its value in an academic journal, Poggendorff's Annalen, in 1860⁴. He measured the viscosity of water with the Hagen-Poiseuille equation⁵ while changing the water temperature. Later, Holman^{6,7} measured the viscosity for various fluids and temperatures by 1886. In 1894, Ostwald⁸ established the method of capillary viscometer, which became commonly used to measure the viscosity of fluids⁹⁻¹⁹.

According to Flower⁹, Kawada¹⁰ and Gupta¹¹, there are four major methods for measuring the viscosity of fluids, i.e. capillary^{12,13}, falling ball/piston^{14,15}, rotational^{16,17}, and oscillating^{18,19} viscometers, and they have been already established by 1914. For example, the time taken for the fluid to flow is measured by a capillary viscometer. Similarly, the torque required to maintain a constant speed is measured by a rotational viscometer, logarithmic decay rate by an oscillating viscometer, and the time taken for an object to pass through by a falling ball/piston viscometer. In total, these conventional methods have a feature that the measured quantity increases with viscosity. It follows that they tend to decrease its measurement accuracy and to require larger equipment for its improvement when the viscosity or shear stress is small, although the tendency does not necessarily make the measurement of viscosity impossible. Furthermore, the viscosity generally depends on physical properties such as shear rate and temperature, which are not uniform inside the finite experimental apparatus. Consequently, the measurement involves errors or the need for corrections based on the condition of the experimental apparatus, posing the problem of determining the temperature, pressure, and shear rate at which the viscosity is measured.

In this study, a new method of FMS (Fluid Mode Spectroscopy) for measuring kinematic viscosity of fluids is proposed based on a spectroscopy that decompose a velocity field into fluid modes, Stokes eigenmodes^{20,21}, with inherent decay rates. The method, regarded as one of mode spectroscopy methods for measuring diffusion coefficients²²⁻²⁵, measures the

(exponential) decay rate of fluid speed after the fluid is stirred, evaluating the viscosity in nearly a spatially uniform, zero-shear-stress, stationary state of the fluid. In principle, it is easy for us to apply the method to fluids with low viscosity, such as water, without corrections by prolonging the measurement time. Its accuracy depends only on the used velocimetry. Inversely, its application to larger viscosity fluids tends to diminish the accuracy because of the measurement of decay rate within a shorter period. In addition, it cannot be utilized as a rheometry, i.e. a viscometry for non-Newtonian fluids under non-zero shear stresses at this time. Instead, direct measurement of the kinematic viscosity at zero shear stress without extrapolation is possible for FMS, while impossible for conventional methods. The proposed method is useful in the sense that FMS and conventional methods complement each other.

In recent years, new methods for the viscosity measurement have been proposed. They include viscometries by using a quartz crystal resonator²⁶, ultrasonic shear-wave reflectance²⁷, an ultrasonic transducer in a reserve tank²⁸, droplet microfluidics²⁹, oscillating drops³⁰, surface distortion caused by a pulsed gas jet³¹, and others^{32–36}. To our best knowledge, however, a spectroscopy decomposing a velocity field into decaying fluid modes has not been utilized as a viscometer. This study is the first trial to apply the method to measuring the viscosity of water in a cylindrical container with a free, top surface, and its applicability and accuracy are investigated.

II. FLUID MODE SPECTROSCOPY (FMS)

A. Fundamentals of FMS

The principle of Fluid Mode Spectroscopy (FMS) is so simple. After a fluid in an open or closed container is stirred to give an initial velocity field \mathbf{v}^* of position \mathbf{x}^* at time $t^* = 0$, the field decays to vanish without forcing. In this study, asterisk $*$ denotes dimensional quantities. The transient field can be typically expressed as the superposition of fluid modes $\mathbf{v}_1^*, \mathbf{v}_2^*, \dots$ as follows

$$\mathbf{v}^*(\mathbf{x}^*, t^*) = e^{-\lambda_1^* t^*} \mathbf{v}_1^*(\mathbf{x}) + e^{-\lambda_2^* t^*} \mathbf{v}_2^*(\mathbf{x}) + \dots, \quad (1)$$

where $0 < \lambda_1^* \leq \lambda_2^* \leq \dots$. Such modes are well known to be the Stokes eigenmodes^{20,21}. The (exponential) decay rate λ_i^* is the real eigenvalue corresponding to the i th eigenvector field

\mathbf{v}_i^* , and \mathbf{v}_1^* is the slowest decaying mode (SDM). Since the RHS of Eq. (1) is dominated by the SDM after sufficiently long time, we can eventually detect the decay rate λ_1^* of \mathbf{v}^* as the gradient on a semi-log plot.

The Buckingham Π theorem leads to that the physical quantities in Eq. (1) are normalized by the kinematic viscosity ν of the fluid and typical length L^* and that the normalized decay rate $\lambda_{SDM}(\equiv \lambda_1^* L^{*2}/\nu)$ of the SDM must depend only on the normalized shape of a fluid container. The rate is obtained by solving a dimensionless eigen equation for the Stokes eigenmodes. For the case of an axisymmetric, radius-component-free flow in a horizontally positioned cylindrical container with a flat upper, open surface, the rate is analytically found to be

$$\lambda_{SDM} = x_1^2 + \left(\frac{\pi}{2\alpha}\right)^2, \quad (2)$$

where $x_1(\doteq 3.83170597)$ denotes the positive, smallest zero of the Bessel function of the first kind of order unity, $J_1(x)$, and α the aspect ratio of depth D^* to the inner radius $R^*(= L^*)$ of the container. The azimuthal velocity component u_θ of its corresponding eigenvector field is of the form

$$u_\theta \sim J_1(x_1 r) \sin\left(\frac{\pi z}{2\alpha}\right) \quad (3)$$

where $r(= r^*/R^*)$ denotes dimensionless radius, and $z(= z^*/R^*)$ dimensionless height. See Appendix A.

Thus, the kinematic viscosity of a fluid in a container can be evaluated by

$$\nu = \lambda_1^* L^{*2} / \lambda_{SDM}, \quad (4)$$

with a measured (dimensional) decay rate λ_1^* . This is the essence of FMS.

Rigorously speaking, the expression (1) makes physical sense for the case that all eigenvalues are semi-simple. Since the negative gradient of $\ln(t^b \exp(-\lambda_{SDM}t))$ is well approximated by λ_{SDM} for a constant b , even if not so, the value of λ_{SDM} , whether obtained analytically or numerically, makes it possible for us to utilize the method of FMS.

In order to avoid numerical errors, it is desirable that λ_{SDM} is obtained analytically. Moreover, the area of flow visualization can be limited to the top surface for measuring the

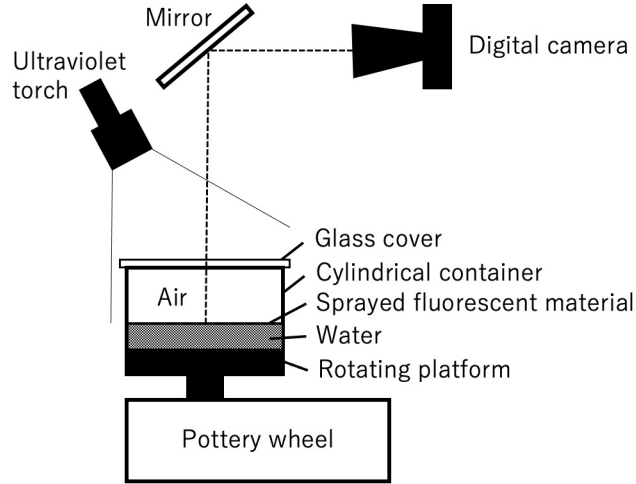


Figure 1. Experimental setup

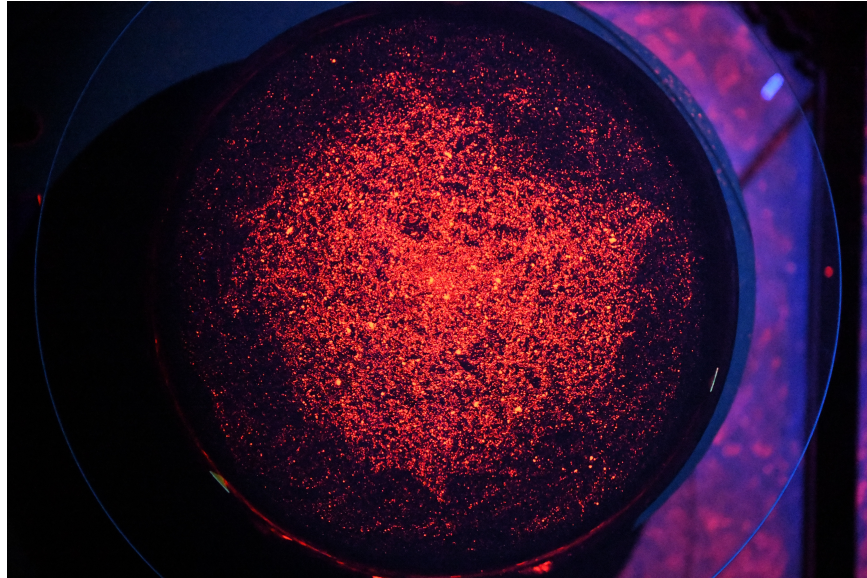


Figure 2. An example of a photo of a fluorescent top surface, illuminated by an ultraviolet torch.

decay rate λ_1^* for the case of an open container. They are the reason why we conducted experiments by use of an open cylindrical container described in the next section.

B. Experimental procedure

The experimental setup of this study is shown in Fig. 1. Water was poured by the depth of 8.0 cm into a horizontally-positioned, acrylic and open cylindrical container with the inner diameter of 29 cm, and a solution (specific gravity: 0.94-0.95) of 11.6 wt% fluorescent

material (Central Techno, Lumisis E-420) for ultraviolet laser-induced fluorescence in predominantly oleic acid-based oil was sprayed one time on the top water surface by a small atomizer so that the droplets of the oil were distributed as uniformly as possible. The light of peak wave length 613 nm is emitted by the material, excited by the ultraviolet light of wave length between approximately 250 and 380 nm. The use of ultraviolet light prevents photos from halation, while the visible light emission from the fluorescent material makes the visualized flow clearer, suitable for low-speed PIV (Particle Image Velocimetry).

The temperature of water was measured two times by a thermistor (Netsuken, SN3000) before and after an experiment. The (absolute) difference of the two temperatures exceeds 0.4 °C for only 4 cases in total 67 experiments in this study, being within 0.1 °C for 42 cases. The arithmetic mean of the temperatures was utilized to evaluate the viscosity of water. The mean temperature at each experiment ranges from 9.0 to 27.5 °C. As a result, the kinematic viscosity of the water^{37,38} changes from 8.465×10^{-7} to 1.351×10^{-6} m²/s, and just the variation simulates the assessment with the exchange of low-viscosity fluids.

After the spray of the solution and the temperature measurement, a glass cover that prevents inner water flow from the disturbance of outer air flow in the laboratory was placed on the container. Although an air layer of the depth of 3.0 cm ($\equiv D^{*}$) is made between the cover and the water surface, an accurate measurement of slow speed on the surface was impossible without the cover.

After that, the container was horizontally rotated at a fixed speed for ten minutes by an electric pottery wheel (Nidec-Shimpo, RK-3D), and an axisymmetric flow was induced. The speed was also not fixed: the maximum value of top-surface-mean speed ranges from 1.421×10^{-3} to 2.057×10^{-3} m/s. After the cease of the rotation, the top moving surface of the container, illuminated by an ultraviolet torch (Central Techno, YKD-200, peak wave length: 365 nm) in a darkened room, was shot by a digital camera (Nikon, D850, total pixels of the image sensor: 46.89 million) with an aspherical, low-distortion lens (Nikon, AF-S NIKKOR 24-70mm f/2.8E ED VR) every two seconds for an hour. Such a long sampling, for about 0.2 in dimensionless time, was required because of the low kinematic viscosity of the water. Each photo, an example is shown in Fig. 2, has 5408 by 3600 pixels, taken at the focal length of 105 mm. The time-lapse movie, whose distortion is to be calibrated by a photo of a check pattern, was processed by a PIV analyzer (Kato Koken, Flow Expert2D2C) and the velocity field on the top surface was obtained. The time variation of its mean speed was

utilized to evaluate the decay rate of SDM.

C. Standard and pseudo SDMs and classification scheme

The evaluation of kinematic viscosity based on Eqs. (2) and (4) assumes that the open, top surface of a cylindrical container is kept flat during an experiment. Since the top surface is well approximated by the flat one after sufficiently long time, it is certain that there exists the SDM described in Sec. II A, hereafter referred to as the standard SDM.

When a fluid speed is relatively large, however, the effect of a surface wave, sloshing, is not negligible. An irrotational, (almost) inviscid, linear wave theory deduces that the sloshing in a cylindrical container has the SDM of a dimensionless decay rate $2x_1^2 (\equiv \lambda_{SDM}^{(s)})$ with the distribution of azimuthal velocity component being the Bessel function³⁹. The rate is independent of the aspect ratio α , caused by the linear-, infinitesimal-amplitude-wave theory that neglects the effect of viscosity near wall surfaces. After a long time, the effect has the fluid motion approached the standard SDM asymptotically. The temporal, pseudo SDM is referred to as the sloshing SDM.

In order to measure the kinematic viscosity using such an open container, it is crucial to properly classify each vanishing fluid mode into one of the SDMs. The standard mode is observed when an initial surface wave on the top surface, associated with initial fluid speed, is small enough so that after a short period the distribution of azimuthal velocity component is well approximated by the Bessel function. Such time evolution is realized when the top surface is kept flat. Inversely, the sloshing mode is observed when the initial speed is large enough to actualize the initial wave. Note that physically high or low speed depends on the kinematic viscosity of a test fluid. It is reasonable, therefore, that we introduce a dimensionless criterion U_c to determine whether or not the initial speed, say the maximum dimensionless top-surface-mean speed U_{max} , is high enough for producing initial waves.

Once such a wave occurs, it takes much time to appear the Bessel-like azimuthal distribution even if the initial speed is relatively low. The experimental observation makes it virtually impossible to obtain the decay rate λ_{SDM} of the standard SDM within the accuracy of velocimetry. Therefore, the condition that the azimuthal distribution is well approximated by the Bessel function, i.e. the correlation coefficient c between the distribution and a correlation Bessel function is larger than a criterion c_c , at a certain time t_c after a long time

must be a necessary condition for the standard SDM.

Herein, we should note that the sloshing SDM is observed while the surface wave is large enough. Eventually, such a wave is affected by the viscous boundary layer in the vicinity of wall surfaces, and the dimensionless decay rate is apart from $\lambda_{SDM}^{(s)}$. When $U_{max} < U_c$, therefore, the fluid mode can not be regarded as the sloshing SDM even if $c \leq c_c$.

Furthermore, we need a sufficiently long, straight-line, dimensionless time range T_{sl} on a semi-log plot of dimensionless relation between top-surface-mean speed U and time t for evaluating the decay rate accurately, regardless of whether or not a mode is the standard SDM.

That is the reason why experimental vanishing fluid modes are classified as follows. A mode is the standard SDM if

$$U_{max} < U_c, T_{sl} \geq T_c, \text{ and } c > c_c \text{ at } t = t_c, \quad (5a)$$

and the sloshing SDM if

$$U_{max} \geq U_c \text{ and } T_{sl} \geq T_c, \quad (5b)$$

and otherwise discarded.

III. RESULTS AND DISCUSSIONS

The classification fully depends on the dimensionless critical values. Firstly, the instant t_c is set at 0.1, i.e. $t_c^* = 2103$ s when a water temperature is 20 °C, so that the time is more than twice as large as the decay time of $1/\lambda_{SDM}$ ($= 0.044$) and at the instant the top-surface-mean speed U , estimated at $23.8 (= \bar{U}_{max} \exp(-\lambda_{SDM} t_c))$, is greater than the dimensionless speed-measurement limit of 10.7-17.1, estimated from a typical dimensional limit of 0.1 mm/s, where in this study the mean value \bar{U}_{max} of U_{max} is 232.0. In addition, c_c and T_c are fixed at 0.995 and 0.06, respectively. The pseudo, sloshing mode eventually agrees with the standard one, therefore the criterion c_c must be relatively higher value to distinguish these modes with each other. The T_c corresponds to 1262 s when a water temperature is 20 °C. Although the accuracy of the decay rate increases with T_c , the number of classified SDMs decreases. In this study, the average of T_{sl} for total 67 cases is 0.0737, and such a smaller critical value ensures a sufficient number of SDMs. In contrast, the reasoning of the critical

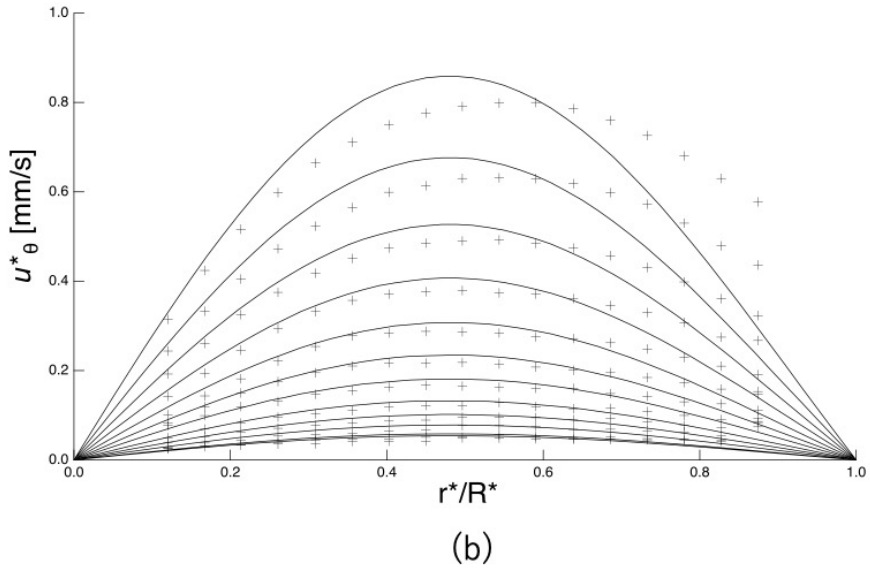
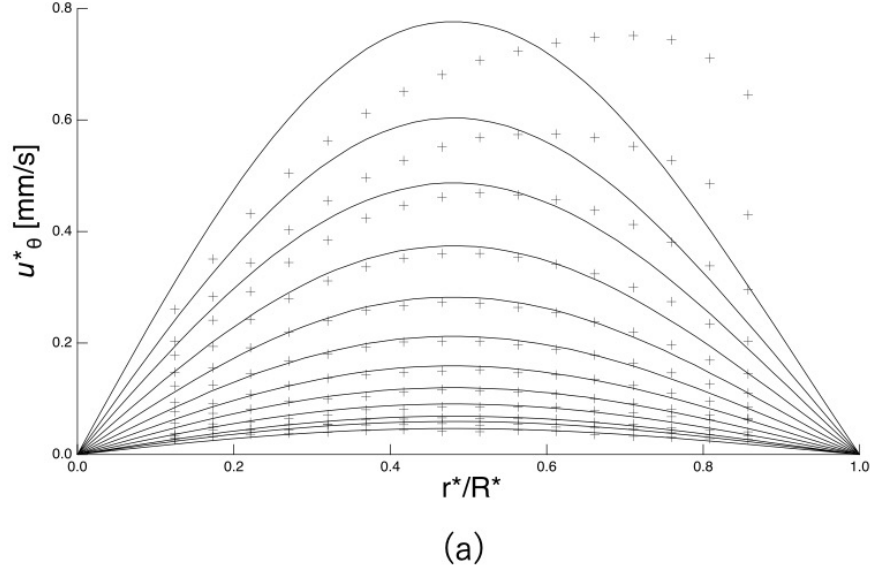


Figure 3. Typical distributions of azimuthal velocity component for (a) the standard and (b) sloshing SDMs, drawn every 200 s from $t^* = 1000$ to 3200 s. The measured distributions and their corresponding correlation Bessel functions are indicated by markers and solid lines, respectively. The uppermost is at $t^* = 1000$ s.

value U_c is impossible. Therefore, the value must be treated as a parameter. Taking \bar{U}_{max} into consideration, therefore, we switched the value between 223 and 240, and the effects on evaluated viscosity are examined.

Typical distributions of azimuthal velocity component are shown in Fig. 3. Fig. 3(a) shows an example (case A) of the distribution of the standard SDM. In this case, the water

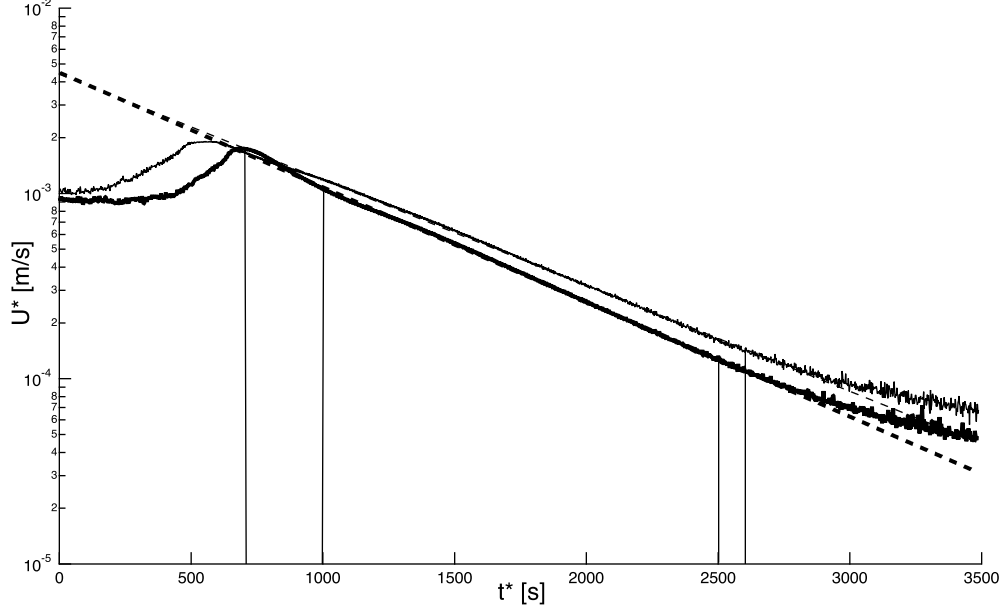


Figure 4. Time variation of top-surface-mean speed. Thick and thin solid lines indicate the variation for cases A and B, respectively. Vertical lines show the region of straight line on the semi-log plot, and two dashed lines show the corresponding results of exponential fitting.

temperature is $12.2\text{ }^{\circ}\text{C}$, and U_{max} , U_{max}^* , T_{sl} and c at $t = 0.1$ are 2.07×10^2 , 1.76 mm/s , 8.80×10^{-2} and 0.998 , respectively. The distribution is well approximated by the Bessel function with a slight difference near the side wall in the sense that the correlation coefficient between the distribution and the function exceeds 0.998 for $t^* \geq 1800$ ($t > 0.1$). On the other hand, Fig. 3(b) is an example (case B) of the distribution of the sloshing mode. The water temperature of the case is $25.1\text{ }^{\circ}\text{C}$, and U_{max} , U_{max}^* , T_{sl} and c are 3.11×10^2 , 1.91 mm/s , 8.07×10^{-2} and 0.983 , respectively. While the distribution is lower at the center, it is higher near the side wall, when compared to correlation Bessel functions. These figures show that c_c must be over 0.99 for apparent agreement with the Bessel function.

The corresponding variations of top-surface-mean speed are shown in Fig. 4. We can confirm that there exist linear regions between corresponding two vertical lines on the semi-log plot and that each region is well approximated by the corresponding exponential function. It should be noted that the exponential decay begins even when the distribution of azimuthal velocity component is far from the Bessel function in comparison with Fig. 3. The property allows us to evaluate the exponential decay rate accurately.

Similarly, the exponential decay rates for the other cases are evaluated and normalized by

Table I. Average of normalized decay rates and their standard deviation for each mode. The critical value U_c is changed from 223 to 240.

U_c	223		240	
slowest decaying mode (SDM)	standard sloshing		standard sloshing	
data number	6	21	10	13
analytical decay rate (λ_{SDM} or $\lambda_{SDM}^{(s)}$)	22.8	29.4	22.8	29.4
mean decay rate $\bar{\lambda}$	23.9	29.5	23.7	32.1
unbiased variance V	3.68	32.3	7.39	24.2
standard deviation $\sigma(= \sqrt{V})$	1.92	5.69	2.72	4.92
relative error to analytical value ($= \sigma/\lambda_{SDM}^{(\bullet)}$)	0.084	0.194	0.119	0.168

the kinematic viscosity at each water temperature. The total result of uncertainty analyses is shown in Table I.

Firstly, it is found that the theoretical decay rates λ_{SDM} and $\lambda_{SDM}^{(s)}$ are included in the average value $\bar{\lambda}$ of decay rates \pm its standard deviation σ for each SDM, i.e. $|\bar{\lambda} - \lambda_{SDM}| < \sigma$, indicating that the classification of the two modes is appropriate. Under the condition that the relation holds and that ν is constant, the relative error of measured kinematic viscosity ν_m , estimated by Eq. (4), to the real value ν is bounded above by that of dimensionless decay rate λ to λ_{SDM} because of the following inequality

$$\left| \frac{\bar{\lambda}}{\lambda_{SDM}} - 1 \right| = \left| \frac{\bar{\lambda}^* L^2 / \nu}{\bar{\lambda}^* L^2 / \bar{\nu}_m} - 1 \right| = \left| \frac{\bar{\nu}_m}{\nu} - 1 \right| \leq \frac{\sigma}{\lambda_{SDM}}. \quad (6)$$

It follows that the relative error of measured kinematic viscosity with the temperature of a test fluid fixed by a thermostat under a constant ambient pressure is less than or equal to the relative error shown in Table I. Recall that dimensionless properties obtained by experiments are independent of a kind of fluid.

The deviation σ , i.e. error, of dimensionless decay rate for the standard SDM, is always smaller than that for the sloshing SDM, independent of U_c . It follows that relatively accurate measurement can be achieved by use of the standard SDM.

We can also find that the error for the standard SDM increases with U_c and that more accurate measurement can be conducted by diminishing an initial speed. In order to take a longer T_{st} , however, more accurate velocimetry should be utilized. In Fig. 4, the measured

speed is apart from the exponential correlation function and begins to fluctuate when the speed is below 0.1 mm/s ($\equiv u_{lim}^*$), at which it reaches the limit of measurement. The condition (5a) for the standard SDM leads to

$$U_c e^{-\lambda_{SDM} T_c} > U_{max} e^{-\lambda_{SDM} T_{sl}} > u_{lim}.$$

In order to ensure a sufficient data number of the standard SDM, $u_{lim}/U_c (= u_{lim}^*/U_c^*)$ must be small enough when compared to $\exp(-\lambda_{SDM} T_c)$. If we can reduce u_{lim} to half, we can also reduce U_c to half with T_c fixed, and it contributes to more accurate measurement by the standard SDM.

In contrast, the error for the sloshing SDM decreases with U_c . However, it is insufficient for accurate measurements. As long as an initial speed is large enough, the sloshing SDM occurs frequently and makes it possible for us to measure easily the kinematic viscosity with lower accuracy. For example, the method can be utilized for a device to notify the necessity of the exchange of machine oil.

Finally, it is proper to point out that the increase of the mean decay rate up to 0.2–0.4 for the standard mode can be explained by the glass cover. In fact, axisymmetric, radial-component-free, two-dimensional simulations in a closed cylindrical container with the air and water layers coupled, their interface kept flat, and the depth ratio D^*/D^* fixed at 3/8 show that the dimensionless decay rate of the SDM changes from 23.0 (5°C) to 23.2 (30°C). Although the details are omitted in this paper, the ratio of the dynamic viscosity of air to that of water, i.e. $1.15 \times 10^{-2} - 2.35 \times 10^{-2}$ for 5 – 30°C, convinces us of the rate increase. The deviation about 0.3 from the analytical value 22.8 and its dispersion ± 0.1 are far smaller than the standard deviation σ , which is greater than 1.92. Similarly, the effect of the cover on the decay rate of the sloshing SDM is expected to be the order of 1%. The advantage of the cover in the reduction of σ surpasses the disadvantage in this study.

IV. CONCLUDING REMARKS

This study presents a new method to measure accurately the kinematic viscosity of fluids by use of a spectroscopy decomposing a stirred, vanishing velocity field into fluid modes (Stokes eigenmodes). The method, Fluid Mode Spectroscopy (FMS), is based on the fact that each Stokes eigenmode has its inherent decay rate of eigenvalue and that the dimension-

less rate of the slowest decaying mode (SDM) is constant, dependent only on the normalized shape of a fluid container. The decay rate is obtained analytically for some shapes like an open cylindrical container of this study. The FMS supplements major conventional measuring methods with each other, particularly useful for measuring low kinematic viscosity. The main results are as follows:

1. In order to avoid numerical errors for evaluating λ_{SDM} and to use easier flow visualization, an open cylindrical container of this study was the best. However, an open container involves a pseudo, sloshing decay mode. Therefore, we have no choice but to classify each vanishing fluid mode into the mode and a viscous, surface-flat standard mode.
2. The classification depends on four dimensionless criteria, i.e. the maximum velocity U_c , linearly time range T_{sl} on semi-log plot of the relation between the surface-averaged speed and time, and correlation coefficient c_c between a distribution of azimuthal velocity component and its correlation Bessel function at an instant t_c .
3. By use of the standard mode in an open cylindrical container the kinematic viscosity of water is measured within a relative error smaller than 8.4-11.9%. Taking that water is a typical example of low-viscosity fluids into consideration, the measurement is accurate. The smaller U_c , more accurate the measurement becomes. Since the value is proportional to a lower limit of velocity measurement, the accuracy fully depends on the used velocimetry.
4. By use of the sloshing mode, the kinematic viscosity is measured within a relative error smaller than 16.8-19.4%. The mode is frequently observed when an initial speed is high enough, useful for easier, low-precision measurements, such as a device to notify the necessity of the exchange of machine oil.
5. Thus, within the error of each vanishing fluid mode, the applicability and methodology of FMS are validated.

In principle, the method is applicable to any type of fluid whose visualization is possible. In order to increase initial speed and S/N ratio thereby, the measurement must be ultimately classification-free. It virtually makes the critical value U_c infinity, and we can take a sufficiently large U_{max} for an experiment based on the standard SDM. There are two methods

for the purpose. One is the method to utilize a closed container. For example, we can analytically obtain λ_{SDM} even if a cylindrical container is closed, as described in the next section. The rate allows us to apply FMS to closed cylindrical containers. The other is the method to equate the decay rate λ_{SDM} of the standard SDM with that of the sloshing mode, $\lambda_{SDM}^{(s)}$. It is achieved when the aspect ratio α of the fluid layer in a cylindrical container is equal to $\pi/(2x_1)$.

The effects of other parameters on the accuracy of FMS are of interest. For example, the mere asperity, roughness, of a container is expected not to affect the accuracy, because the thickness of a velocity boundary layer on a wall surface reaches the order of the radius or depth of the container after a long time. However, if the wall is made by a porous media, its macroscopic skin friction may be quantified by the decay rate of FMS. They are issues in the future.

ACKNOWLEDGMENTS

HI is grateful to M. Miyahara and M. Suzuki of Central Techno corporation for providing the technical information of the solution of fluorescent material in oil. HI is also grateful to Dr. Y. Ueda of Setsunan University for enlightening discussions on the possible modes in open cylindrical containers.

AUTHOR DECLARATIONS

Intellectual property

HI, NI, TH, and AK have a pending patent (publication number: JP, 2021-063675, A) for FMS. MH has a licensed Japanese patent (No. 6713598) for the fluorescent material utilized in this experimental study.

DATA AVAILABILITY

The data that supports the findings of this study are available within the article.

Appendix A: Axisymmetric, radius-component-free Stokes eigenmodes in cylindrical containers

Now let us consider axisymmetric Stokes eigenmodes in horizontally positioned cylindrical containers with flat top and bottom faces. Particularly, we shall confine to the discussion for the case that the radius component u_r of velocity is zero in this section. The condition allows us to decouple the pressure term from the Navier-Stokes equation system on the cylindrical coordinates. The dimensionless eigen equation for u_θ , normalized by the kinematic viscosity ν and the inner radius R^* , is of the form

$$-\lambda u_\theta = \frac{\partial}{\partial r} \left(\frac{\partial u_\theta}{\partial r} + \frac{u_\theta}{r} \right) + \frac{\partial^2 u_\theta}{\partial z^2},$$

and it is straightforward to solve the equation by the method of separation of variables.

If the flat, top surface is open, free-slip condition $\partial u_\theta / \partial z = 0$ is subjected to the top surface, while no-slip condition, $u_\theta = 0$, is exerted on the bottom ($z = 0$) and side ($r = 1$) walls and on the axis ($r = 0$). Then, the Stokes eigenmodes and their corresponding eigenvalues are found to be

$$u_{\theta(n,m)} \sim J_1(x_n r) \sin \left(\frac{2m+1}{2\alpha} \pi z \right),$$

and

$$\lambda_{n,m} = x_n^2 + \left(\frac{2m+1}{2\alpha} \pi \right)^2,$$

respectively, where the solution is labeled by a positive integer n and a nonnegative integer m , and a relation $A \sim B$ indicates that A is proportional to B . J_1 is the Bessel function of the first kind of order unity, x_n ($n = 1, 2, \dots$) positive n th zero of the function. It follows that the slowest decaying mode and its corresponding eigenvalue can be expressed as Eqs. (3) and (2), respectively.

On the other hand, if all faces are closed, i.e. if no-slip condition is also exerted on the top face, then the solution can be expressed as

$$u_{\theta(n,m)} \sim J_1(x_n r) \sin \left(\frac{m\pi z}{\alpha} \right),$$

and

$$\lambda_{n,m} = x_n^2 + \left(\frac{m\pi}{\alpha}\right)^2,$$

where integers n, m are positive. In this case, therefore, the smallest decay rate $\lambda_{SDM} = x_1^2 + (\pi/\alpha)^2$.

Appendix B: Numerical simulations in cylindrical containers with a flat, open top surface

In this study numerical simulations were also conducted in order to validate the standard SDM of the eigenmode (3) with the eigenvalue (2), and to examine properties when the top free-surface is always flat. Dimensionless and incompressible Navier-Stokes equation system without forcing on the cylindrical coordinates is discretized by finite volume method.

No-slip boundary condition, $\mathbf{v} = \mathbf{0}$, is subjected to the side ($r = 1$) and bottom ($z = 0$) wall surfaces, and periodic condition is exerted on the faces at $\theta = 0$ and 2π . The other faces are subjected to free-slip conditions in the sense that

$$\frac{\partial u_r}{\partial z} = \frac{\partial u_\theta}{\partial z} = u_z = 0 \text{ at } z = \alpha,$$

and that

$$u_r = u_\theta = \frac{\partial u_z}{\partial r} = 0 \text{ at } r = 0.$$

Convection and diffusion terms are discretized by QUICK and central difference schemes, respectively. The differenced equation system is timely evolved by explicit SMAC method. A division number N in the radius ($0 \leq r \leq 1$), azimuth ($0 \leq \theta \leq 2\pi$) and height ($0 \leq z \leq \alpha$) directions is held fixed at 30 except for the case of accuracy assessment.

Firstly, let us consider the problem of whether the standard SDM (3) is the true SDM. Numerical eigenvalue analyses of the Stokes eigenmodes with the aid of the above-mentioned numerical integration were performed for two axisymmetric initial velocity fields as follows:

$$(\text{case } "u_r = 0") \mathbf{v}_0 \equiv (u_r|_{t=0}, u_\theta|_{t=0}, u_z|_{t=0}) = (0, 4ar(1-r)z^2, 0),$$

$$(\text{case } "u_\theta = 0") \mathbf{v}_0 = (-a \sin(2\pi z) \sin(\pi r), 0, a \sin(2\pi r) \sin(\pi z)).$$

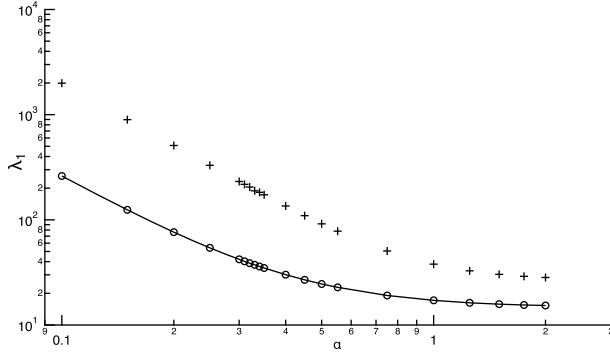


Figure 5. Variation of the smallest eigenvalue λ_1 with respect to α . Solid line is analytical eigenvalue (2). Circle and cross indicate eigenvalues for the cases of “ $u_r = 0$ ” and “ $u_\theta = 0$ ”, respectively. The eigenvalue of the u_r -free mode, less than that of the u_θ -free mode, agrees with that of the standard mode, Eq. (2), and the corresponding distribution, omitted due to space constraints, also agrees with that of the standard mode (3).

The SDM and its corresponding eigenvalue were computed by adjusting the norm of a vector field to unity at each time step. The steady vector field and its corresponding negative increasing rate of the norm before the adjustment at each step agree with the SDM and its corresponding eigenvalue, respectively. Note that, therefore, the magnitude a does not affect the result. It is well known that eigenvector fields of vorticity for the Stokes eigenmode are normal to each other, and therefore we must have different SDMs for the two cases.

The variation of the smallest eigenvalue with respect to the aspect ratio α of the fluid layer are shown in Fig. 5. As expected, two different SDMs are obtained for each initial velocity. However, the eigenvalue of the case “ $u_\theta = 0$ ” is always larger than that of the u_r -free, standard mode, Eq. (2). Particularly, for the case $\alpha \leq 0.32$, the eigenmode for the case “ $u_\theta = 0$ ” is transient, remaining for a finite period of time and eventually shifting to the other SDM. That is to say, the u_θ -free mode is linearly unstable, and the transition is caused by round-off errors involved in numerical simulations. These results indicate that the standard SDM is the true SDM for $0.1 \leq \alpha \leq 2$, computed in this study.

Similar to the u_r -free mode, λ_1 of the u_θ -free mode behaves like $\sim \alpha^c$ when α is small enough with a power low exponent c being slightly smaller than that of the u_r -free mode, and saturates for larger values. It implies that the standard SDM is the true one for any positive α . We can also ascertain that the slowest decaying mode is really axisymmetric,

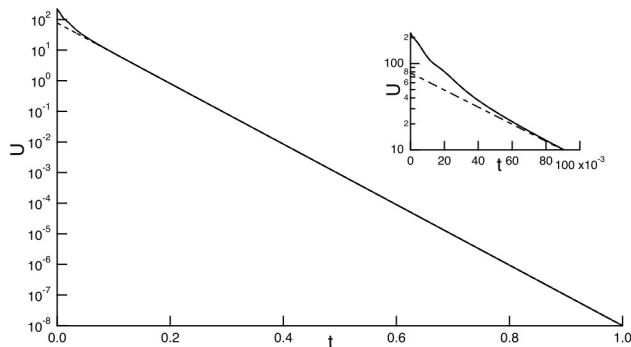


Figure 6. Variation of top-surface-mean speed with respect to time t . The magnification is at around $t = 0$. Dotted and solid lines indicate the variations for $N = 20$ and 30 , respectively. But they are overlapped. For $t > 0.059$ the solid line agrees well with its exponential correlation function, indicated by dashed line, and recovers the decay rate of $22.788(=\lambda_{SDM})$ with the relative error of 0.0092% .

u_r -free one (3) even for a general, non-axisymmetric case of the form

$$\mathbf{v}_0 = (-a \sin(2\pi z) \sin(\pi r), 4ar(1-r)z^2 + a \sin(b\theta), a \sin(2\pi r) \sin(\pi z)),$$

and they are the pieces of numerical evidence that the standard SDM (3) is the true SDM.

Next, common numerical integration without norm adjustment was conducted with an initial axisymmetric velocity field of the form $\mathbf{v}_0 = (0, r\omega, 0)$ except for the no-slip surfaces, where $\omega = 348$ so that the initial top-surface-mean speed would be 232. The aspect ratio α was held fixed at 0.5517. Such an initial velocity distribution, rigid-body rotation, mimics typical experimental one of this study.

The time variations of top-surface-mean speed U and that of the distribution of azimuthal velocity component for $N = 30$ are shown in Figs. 6 and 7, respectively. They show that the exponential decay with the rate of λ_{SDM} begins at around $t = 0.059$, even when the distribution of azimuthal velocity component is far from the Bessel function. The onset of the Bessel-like azimuthal distribution appears at $t = 0.1451$, where the correlation coefficient c is 0.99. The coefficient is raised up to 0.995 at $t = 0.1579$.

In this study the instant t_c at which a decaying mode is classified is set at 0.1, less than 0.1579. But the above-mentioned results depend on an initial velocity distribution \mathbf{v}_0 . For example, for $\omega = 25$ we can confirm that c reaches 0.995 at $t = 0.0814$. Actual initial distributions are far from the rigid-body rotation, dependent on a water temperature and a

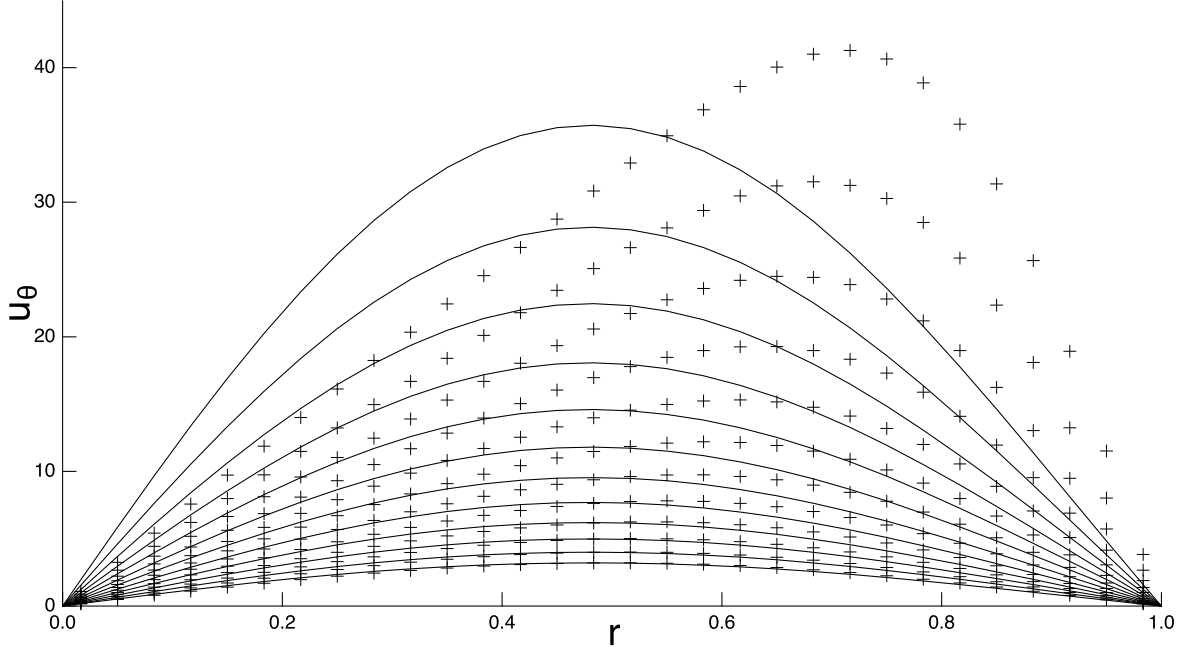


Figure 7. Decays of the distribution of azimuthal velocity component from $t = 0.05$ to 0.16 ($N = 30$). The distribution and its corresponding correlation Bessel function are indicated by plus marker and solid line, respectively. The uppermost is at $t = 0.05$, and time increments are 0.01 . The lowermost distribution agrees well with the Bessel function: the correlation coefficient exceeds 0.995 at $t = 0.16$.

rotational number of each experiment. Moreover, note that the maximum speed at $t = 0.16$, shown in Fig. 7, is much smaller than $10.7\text{-}17.1$, estimated from a typical dimensional measurement limit of 0.1 mm/s. In contrast, the top speed is maintained at around the limit at $t = 0.1$. It is reasonable, therefore, that t_c is fixed at 0.1 in this study.

Although the presentation of the results is omitted due to space constraints, it is easy to perform computations with more different initial conditions for the same aspect ratio α . The results show that the exponential decay begins at $t \simeq 0.06$, independent of an initial velocity distribution \mathbf{v}_0 , because higher modes decays within $t \leq 1/\lambda_{SDM} = 0.044$.

REFERENCES

- ¹C. Gallegos, ed., *Rheology: encyclopaedia of life support systems*, Vol. 1 (Eolss Publishers, 2010) pp. 74–95.

- ²C. L. M. H. Navier, Mem. Acad. Sci. Inst. France **6**, 389 (1822).
- ³G. G. Stokes, Trans. Cambridge Phil. Soc. **8**, 287 (1845).
- ⁴E. Hagenbach, Poggendorff's Annalen **109**, 385 (1860).
- ⁵S. P. Sutera and R. Skalak, Annu. Rev. Fluid Mech. **25**, 1 (1993).
- ⁶S. W. Holman, London Edinburgh Philos. Mag. J. Sci. **3**, 81 (1877).
- ⁷S. W. Holman, London Edinburgh Philos. Mag. J. Sci. **21**, 199 (1886).
- ⁸W. Ostwald, *Manual of physico-chemical measurements* (Macmillan and Company, 1894) pp. 162–168.
- ⁹A. E. Flowers, *Viscosity Measurement and a New Viscosimeter* (Cornell university, 1914).
- ¹⁰M. Kawada, *Viscosity*, Measurement Control Techniques Library, Vol. 1 (CORONA Publishing, Co. Ltd., 1958) (in Japanese).
- ¹¹S. Gupta, *Viscometry for liquids*, Springer Series in Materials Science, Vol. 194 (Springer, 2014).
- ¹²E. Lee, B. Kim, and S. Choi, Sens. Actuator A-Phys. **313**, 112176 (2020).
- ¹³Z. F. Zhang, Euro. J. Phys. **41**, 065803 (2020).
- ¹⁴I. Akhllis, M. Syaifurrozaq, P. Marwoto, R. Iswari, *et al.*, J. Phys.: Conf. Ser. **1567**, 042102 (2020).
- ¹⁵R. Biswas, D. Saha, and R. Bandyopadhyay, Phys. Fluids **33**, 013103 (2021).
- ¹⁶Y. Wang, Z. Liu, L. Cao, B. Blanpain, and M. Guo, Chem. Eng. Sci. **207**, 172 (2019).
- ¹⁷H. J. Skadsem and A. Saasen, Appl. Rheol. **29**, 173 (2019).
- ¹⁸Z. Song, L. Zhang, and H. Ban, Meas. Sci. Technol. **30**, 115903 (2019).
- ¹⁹I. Elyukhina and A. Vikhansky, Measurement **206**, 112267 (2023).
- ²⁰E. Leriche, P. Lallemand, and G. Labrosse, Appl. Numer. Math. **58**, 935 (2008).
- ²¹G. Labrosse, E. Leriche, and P. Lallemand, Theor. Comput. Fluid Dyn. **28**, 335 (2014).
- ²²A. Migliori, J. Sarrao, W. M. Visscher, T. Bell, M. Lei, Z. Fisk, and R. Leisure, Physica B **183**, 1 (1993).
- ²³H. Ogi, H. Ledbetter, S. Kim, and M. Hirao, J. Acoust. Soc. Am. **106**, 660 (1999).
- ²⁴H. Ogi, T. Ishihara, H. Ishida, A. Nagakubo, N. Nakamura, and M. Hirao, Phys. Rev. Lett. **117**, 195901 (2016).
- ²⁵H. Ishida and H. Ogi, Philos. Mag. **98**, 2164 (2018).
- ²⁶A. Miranda-Martínez, M. X. Rivera-González, M. Zeinoun, L. A. Carvajal-Ahumada, and J. J. Serrano-Olmedo, Sensors **21**, 2743 (2021).

- ²⁷E. E. Franco and F. Buiochi, *Ultrasonics* **91**, 213 (2019).
- ²⁸T. Yoshida, K. Ohie, and Y. Tasaka, *Ind. Eng. Chem. Res.* **61**, 11579 (2022).
- ²⁹W. Zeng and H. Fu, *Phys. Fluids* **32**, 042002 (2020).
- ³⁰G. Lohöfer, *Int. J. Thermophys* **41**, 30 (2020).
- ³¹A. Savenkov, M. Mordasov, and V. Sychev, *Meas. Tech.* **63**, 722 (2020).
- ³²L. S. Madsen, M. Waleed, C. A. Casacio, A. Terrasson, A. B. Stilgoe, M. A. Taylor, and W. P. Bowen, *Nat. Photonics* **15**, 386 (2021).
- ³³P. Košťál, T. Hofírek, and J. Málek, *J. Non-Cryst. Solids* **480**, 118 (2018).
- ³⁴O. Takeda, M. Yamada, M. Kawasaki, M. Yamamoto, S. Sakurai, X. Lu, and H. Zhu, *ISIJ Int.* **60**, 590 (2020).
- ³⁵J. Kremer, A. Kilzer, and M. Petermann, *Rev. Sci. Instrum.* **89**, 015109 (2018).
- ³⁶M. I. Pryazhnikov, A. S. Yakimov, I. A. Denisov, A. I. Pryazhnikov, A. V. Minakov, and P. I. Belobrov, *Micromachines* **13**, 1452 (2022).
- ³⁷J. Kestin, M. Sokolov, and W. A. Wakeham, *J. Phys. Chem. Ref. Data* **7**, 941 (1978).
- ³⁸JIS Z 8803:2011, “Methods for viscosity measurement of liquid,” Tech. Rep. (Japanese Industrial Standards Association, 2011).
- ³⁹R. A. Ibrahim, *Liquid sloshing dynamics: theory and applications* (Cambridge University Press, 2005).